

Near Field Microwave Holography for Bio-Tissue Imaging

Yoshihiko Kuwahara^{1*}, Kimihito Fujii²

¹Department of Electrical and Electronic Engineering, Shizuoka University, Hamamatsu, Japan

²Division of Breast and Endocrine Surgery, Department of Surgery, Aichi Medical University, Nagakute, Japan

Email: *kuwahara.yoshihiko@shizuoka.ac.jp

How to cite this paper: Kuwahara, Y. and Fujii, K. (2020) Near Field Microwave Holography for Bio-Tissue Imaging. *Open Journal of Medical Imaging*, 10, 143-150. <https://doi.org/10.4236/ojmi.2020.103014>

Received: August 5, 2020

Accepted: August 25, 2020

Published: August 28, 2020

Copyright © 2020 by author(s) and Scientific Research Publishing Inc.

This work is licensed under the Creative Commons Attribution International License (CC BY 4.0).

<http://creativecommons.org/licenses/by/4.0/>



Open Access

Abstract

This study investigated the ability of microwave holography to accurately reconstruct the tissue structure of the human body. Numerical breast and head phantoms were imaged by 3D near-field holography using backscattered waves obtained by a monostatic planar scan. Complex organizational structures have been reconstructed accurately and quickly. In addition, breasts with relatively simple histology could be reconstructed without the matching liquid.

Keywords

Microwave Imaging, Near Field Holography, Bio-Tissue

1. Introduction

Detection technology for breast cancer or brain strokes, based on microwave imaging, has been widely studied because it has no exposure, allows frequent examinations, and is relatively inexpensive as type of equipment [1] [2]. Typical imaging methods include scattering tomography [3], which solves the inverse scattering problem to obtain the complex permittivity distribution in the object, and ultra-wideband (UWB) radar, which evaluates the scattered power distribution in the object using wideband signals [4]. The former has the ability to accurately reconstruct the tissue image. However, it is essential to accurately model an actual measurement system on a computer, and achieving this realistically is difficult [5]. In addition, since the complex permittivity distribution in the tissue is updated by Newton's method, full wave electromagnetic field analysis is repeatedly performed, requiring a significant amount of calculation [6]. Hence, rapid image reconstruction is difficult. Usage of UWB radar for imaging is relatively easy to realize, and clinical trials for breast cancer detection are being

conducted by several research institutions, including my institution. However, the reconstructed image does not reflect the morphology of the tissue [4] [7] [8], thereby making it difficult to clinically determine the presence or absence of cancer. Hence, it has not been put to practical use.

In recent years, research on wavefront reconstruction (direct holography) based on synthetic aperture radar has progressed, and its application to the detection of breast cancer is also being considered [9]. Microwave imaging by direct holography can reconstruct a tissue image, and calibration using a point scattering function [10] does not require accurate modeling of the imaging system on a computer. Moreover, since the image reconstruction processing is based on the Fourier transform, image reconstruction can be performed in a short time close to real time. Since it is based on the Fourier transform, a high frequency is inevitably required due to the sampling theorem in order to achieve high resolution, and there exists the concern of attenuation in a living tissue. However, there are several reports stating that image reconstruction is possible even with a relatively low Signal to Noise Ratio (SNR) [11].

This study presents an image reconstruction algorithm using near-field holographic imaging. Since [9] is based on far-field holographic imaging, the fidelity of the reconstructed image is insufficient despite the use of a matching liquid. In addition, there are no examples of faithful reconstruction of the tissue structure in the skull. We demonstrate that a monostatic radar that captures backscattered waves in a planer scan can accurately reconstruct 3D tissue tomographic images of the breast and head in a short time by the use of near field holographic imaging.

2. Image Reconstruction

2.1. Near Field Microwave Holography for 3D Imaging

The forward problem of the scattering phenomena is expressed by the following Equation (1) using the linear Born approximation.

$$\mathbf{E}^{sc}(\mathbf{r}_p) \approx \iiint_{V_Q} \left[k_s^2(\mathbf{r}_Q) - k_b^2 \right] \hat{\mathbf{G}}(\mathbf{r}_p, \mathbf{r}_Q) \mathbf{E}^{inc}(\mathbf{r}_Q) d\mathbf{r}_Q \quad (1)$$

Here, \mathbf{E}^{sc} , $\hat{\mathbf{G}}$, \mathbf{E}^{inc} , k_s and k_b denote the scattering field, dyadic Green function, incident field, wave number of the object, and that of the background, respectively. Then, V_Q , position vector \mathbf{r}_p and \mathbf{r}_Q denote a volume to be inspected, position of the observation and scattering.

Assuming planar scanning, the contrast distribution of a region represented by a plurality of cross sections parallel to the scanning plane is estimated. $E_j^{sc}(x', y', \omega_l)$, $j = x, y, z$ denotes j -polarization component of the scattering field at \mathbf{r}_p . Each component of the scattered field at $\mathbf{r}_p = (x', y', 0)$ at frequency ω_l is expressed by,

$$E_j^{sc}(x', y', \omega_l) \approx \iiint_{\mathbb{R}^3} f(x, y, z, \omega_l) \cdot \sum_{i=x,y,z} a_i^j(x-x', y-y', z, \omega_l) dx dy dz \quad (2)$$

Here,

$$f(x, y, z, \omega_l) = k_s^2(x, y, z, \omega_l) - k_b^2(z, \omega_l) \quad (3)$$

$$a_i^j(x, y, z, \omega_l) = E_i^{inc}(x, y, z, \omega_l) G_{0i}^j(x, y, z, \omega_l) \tag{4}$$

The two-dimensional Fourier transform on both sides of Equation (2) is

$$E_j^{sc}(k_x, k_y, \omega_l) \approx \int_z \tilde{F}(k_x, k_y, z, \omega_l) \sum_{i=x,y,z} \tilde{A}_i^j(k_x, k_y, z, \omega_l) dz \tag{5}$$

Here, $\tilde{F}(k_x, k_y, z, \omega_l)$ and $\tilde{A}_i^j(k_x, k_y, z, \omega_l)$ are the two-dimensional Fourier transforms of $f(x, y, z, \omega_l)$ and $a_i^j(x, y, z, \omega_l)$. Furthermore, k_x and k_y are the Fourier variables corresponding to x and y .

We approximate the integral in Equation (5) with the discrete sum of z .

$$E_j^{sc}(k_x, k_y, \omega_l) = \sum_{n=1}^{N_z} \tilde{F}(k_x, k_y, z_n, \omega_l) \sum_{i=x,y,z} \tilde{A}_i^j(k_x, k_y, z, \omega_l) \Delta z \tag{6}$$

where, Δz is the distance between two adjacent reconstruction planes. Considering the frequency dependence of the medium, it is assumed that the contrast function can be expressed by,

$$f(x, y, z, \omega) = h(x, y, z) \varphi(\omega) \tag{7}$$

Taking the two-dimensional Fourier transform of (x, y) on both sides of Equation (7) with respect to x and y ,

$$\tilde{F}(\boldsymbol{\kappa}, z, \omega) = \tilde{H}(\boldsymbol{\kappa}, z) \varphi(\omega) \tag{8}$$

where, $\tilde{H}(\boldsymbol{\kappa}, z)$ is the two-dimensional Fourier transform of $h(x, y, z)$ with respect to (x, y) . Writing (6) and (8) for the all measured frequencies provides N_ω equations for each spatial frequency pair $\boldsymbol{\kappa} = (k_x, k_y)$.

$$\begin{cases} y_1 = a_{11}x_1 + \dots + a_{1N_z}x_{N_z} \\ \vdots \\ y_{N_\omega} = a_{N_\omega 1}x_1 + \dots + a_{N_\omega N_z}x_{N_z} \end{cases} \tag{9}$$

Here,

$$y_l = \tilde{E}_j^{sc}(\boldsymbol{\kappa}, \omega_l) \tag{10}$$

$$a_{ln} = \varphi(\omega_l) \sum_{i=x,y,z} \tilde{A}_i^j(\boldsymbol{\kappa}, z_n, \omega_l) \tag{11}$$

$$x_n = \tilde{H}(\boldsymbol{\kappa}, z_n) \tag{12}$$

We obtain the least-squares solution of this system of equations and find $\tilde{H}(\boldsymbol{\kappa}, z_n)$, $n = 1, 2, \dots, N_z$ for each spatial frequency pair $\boldsymbol{\kappa} = (k_x, k_y)$.

2.2. Use of the Measured Point Scattering Function

In general, the incident field and Green's function data are obtained by simulation, but due to modeling and numerical calculation errors, it is difficult to be implemented practically. It has been proposed to obtain products of the incident field and Green's function specific to the measurement system by measuring a known calibration object (CO). This method uses the concept of point scattering function (PSF), in which the response due to an arbitrary target is convolved with the response due to point scatter (CO).

When a sufficiently small non-dispersion medium CO exists at $(0, 0, z_n)$, the

contrast function of Equation (3) is expressed by,

$$E_j^{sc}(x', y', \omega_l) \approx \sum_{n=1}^{N_z} \Delta z_n \iint_{xy} f(x, y, z_n) \cdot E_j^{sc,co}(x' - x, y' - y, \omega_l; z_n) dy dx \quad (15)$$

Therefore, the two-dimensional Fourier transform of $E_j^{sc}(x', y', \omega_l)$, $j = x, y, z$ is expressed by,

$$\tilde{E}_j^{sc}(k_x, k_y, \omega_l) \approx \sum_{n=1}^{N_z} \Delta z_n \tilde{F}(k_x, k_y, z_n) \tilde{E}_j^{sc,co}(k_x, k_y, \omega_l; z_n) \quad (16)$$

$\tilde{E}_j^{sc,co}(k_x, k_y, \omega_l; z_n)$ denotes the two-dimensional Fourier transform of $E_j^{sc,co}(x, y, \omega_l; z_n)$.

Applying Equation (16) to the data at all the frequencies $\omega_l (l = 1, \dots, N_\omega)$, a system of equations at each spatial frequency pair $\boldsymbol{\kappa} = (k_x, k_y)$ is constructed.

$$\begin{bmatrix} \tilde{E}_j^{sc}(\boldsymbol{\kappa}, \omega_1) \\ \vdots \\ \tilde{E}_j^{sc}(\boldsymbol{\kappa}, \omega_{N_\omega}) \end{bmatrix} = \begin{bmatrix} \tilde{E}_j^{sc,co}(\boldsymbol{\kappa}, \omega_1; z_1) \Delta z & \cdots & \tilde{E}_j^{sc,co}(\boldsymbol{\kappa}, \omega_1; z_{N_z}) \Delta z \\ \vdots & \ddots & \vdots \\ \tilde{E}_j^{sc,co}(\boldsymbol{\kappa}, \omega_{N_\omega}; z_1) \Delta z & \cdots & \tilde{E}_j^{sc,co}(\boldsymbol{\kappa}, \omega_{N_\omega}; z_{N_z}) \Delta z \end{bmatrix} \begin{bmatrix} \tilde{F}(\boldsymbol{\kappa}, z_1) \\ \vdots \\ \tilde{F}(\boldsymbol{\kappa}, z_{N_z}) \end{bmatrix} \quad (17)$$

After solving Equation (17) for all values of $\boldsymbol{\kappa}$, the inverse Fourier transform of $\tilde{F}(\boldsymbol{\kappa}, z_n), n = 1, 2, \dots, N_z$ is performed, and the contrast function $f(x, y, z_n)$ is reconstructed.

3. Bio-Tissue Image Reconstruction

Tomographic imaging has been performed on the numerical breast and head phantom using the method detailed in Section 2. The antenna uses a half-wave length dipole, and the length is set to resonate at the center frequency of the band. As shown in **Figure 1**, the imaging system is a monostatic radar that uses the same antenna for reception and transmission, and scans the antenna within a plane facing the measurement target. The resolution of the reconstructed image is 2 mm. The breast phantom was created based on the MRI images of cancer patients. The data from [12] was used for the construction of the head phantom.

3.1. Breast Imaging

The measurement frequency range is 2 - 16 GHz, and the distance between the scanning plane and breast is 50 mm. Scattered fields were obtained in 2 mm

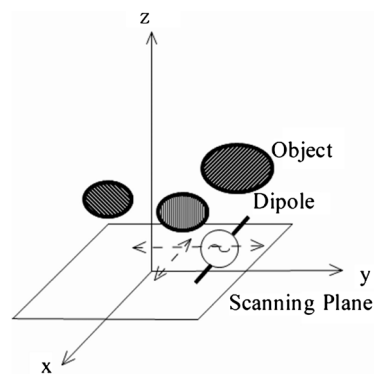


Figure 1. Simulation setup.

steps, within the plane with a 100×100 mm range. The CO has a size, relative permittivity, and conductivity of 2 mm^3 , 25, and 0.75 [S/m] , respectively, and was moved from 3 to 45 mm in steps of 3 mm at $(x, y) = (0, 0) \text{ mm}$ to obtain the measured PSF. Since no matching liquid is used, the relative dielectric constant and conductivity of background set to 1 and 0 [S/m] , respectively.

Figure 2 presents a tomographic image of the real part of the complex permittivity

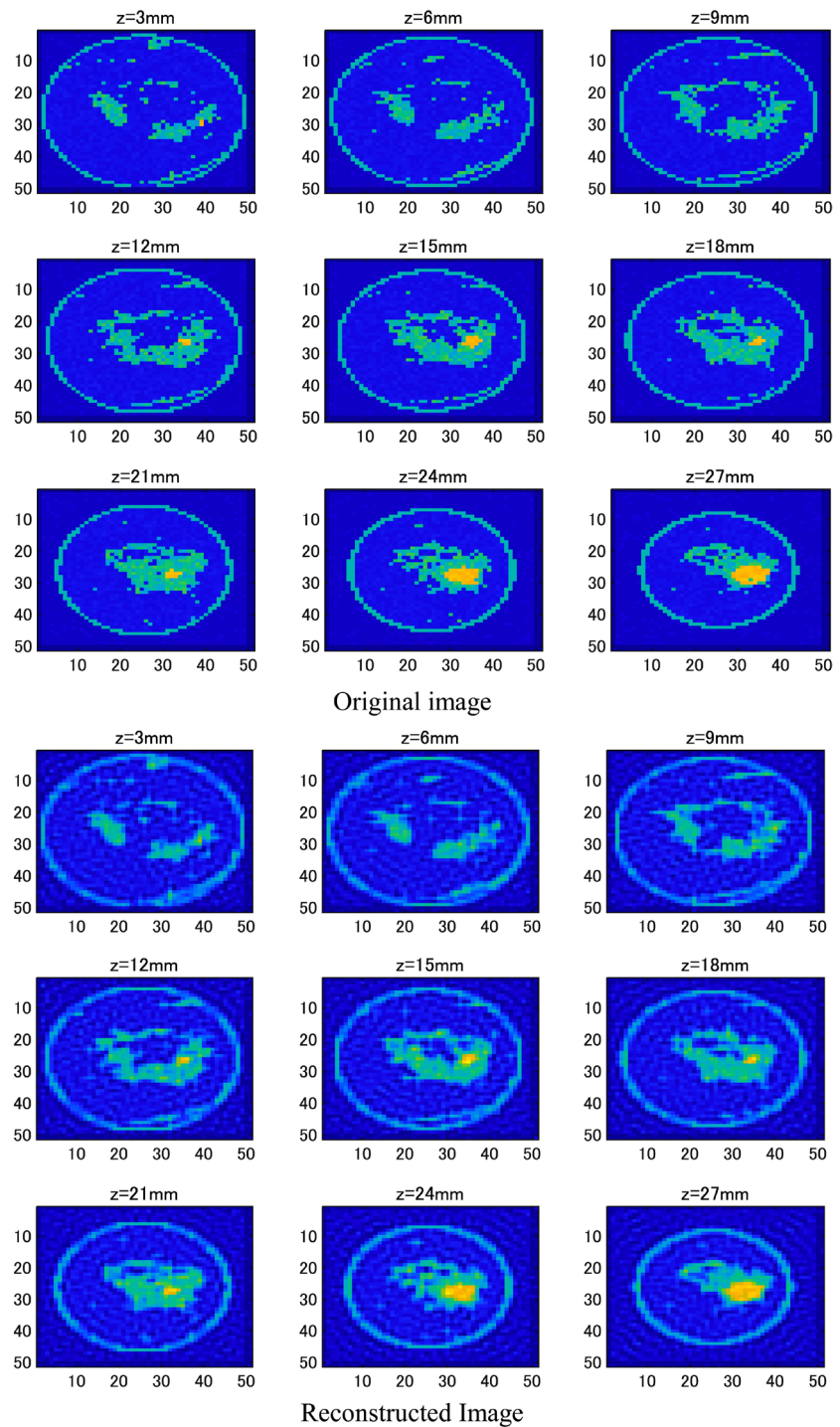


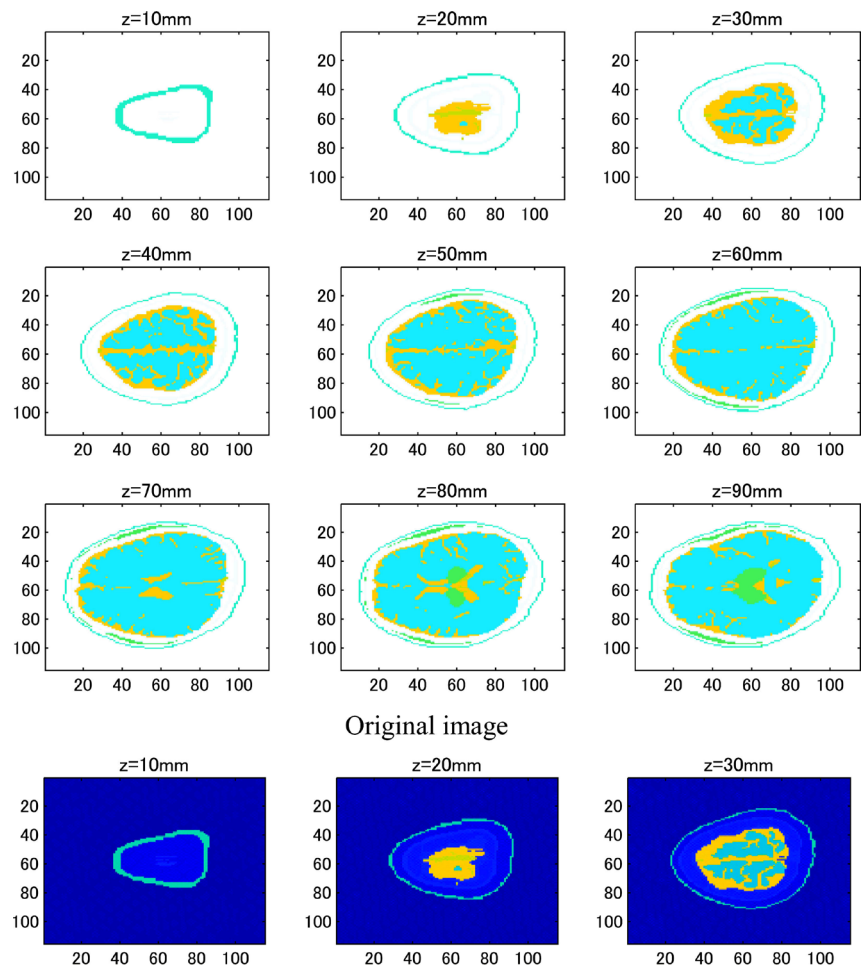
Figure 2. Breast imaging.

of the numerical breast phantom and a reconstructed tomographic image. Despite the absence of matching fluid, the breast tissue structure is accurately reconstructed. The time required for calculation and display of the reconstructed image was only 1.8 s on a personal computer equipped with an i7-6700k CPU and 32GB RAM.

3.2. Head Imaging

The measurement frequency range is 1.1 - 21 GHz and the distance between the scanning plane and head is 50 mm. Scattered fields were obtained in 2 mm steps within the plane, with a 228×228 mm range. The CO with a size, relative permittivity and conductivity of 2 mm³, 60, and 2, respectively, was moved from 2 to 100 mm in 2 mm steps at $(x, y) = (0, 0)$ mm to obtain the measured PSF. In this application, it is difficult to reconstruct the image without the matching liquid. The relative dielectric constant and conductivity of the background was set to 25 and 0.75, respectively.

Figure 3 depicts a tomographic image of the real part of the complex permittivity of the numerical head phantom and a reconstructed tomographic image. The inner tissue of the head is accurately reconstructed. The time required for the calculation and display of the reconstructed image was 7.7 s.



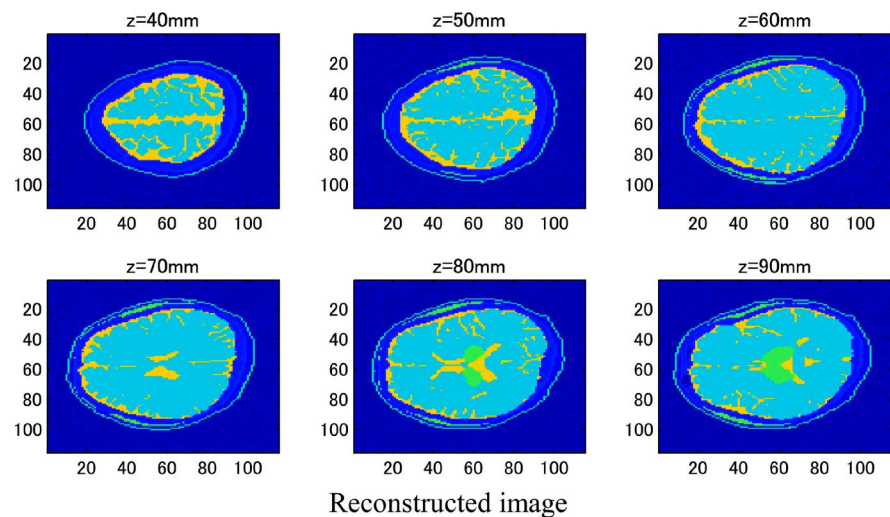


Figure 3. Head imaging.

4. Conclusion

A numerical breast phantom and head phantom were imaged by 3D near field holography using the backscattered waves obtained by the monostatic planer scan. Reconstruction of the complex tissue structure could be accurately and rapidly achieved. In addition, breasts with relatively simple histology can be reconstructed without the matching liquid. Since the image reconstruction in this method is based on the principle of the Fourier transform, it is necessary to acquire wideband scattering data at several observation points. It is difficult to form an array considering the realistic antenna aperture area, and mechanical scanning is a practical concern. Obtaining the data is a time consuming process. Therefore, it must be to examine how to collect the scattering field rapidly. We also need to evaluate the adequacy of applying the Born approximation. While solving these problems, we will continue to develop medical imaging equipment using the microwave holography.

Conflicts of Interest

The authors declare no conflicts of interest regarding the publication of this paper.

References

- [1] Nikolova, N.K. (2011) Microwave Imaging for Breast Cancer. *IEEE Microwave Magazine*, **12**, 78-94. <https://doi.org/10.1109/MMM.2011.942702>
- [2] Mohammed, B.J., Abbosh, A.M., Mustafa, S. and Ireland, D. (2014) Microwave System for Head Imaging. *IEEE Transactions on Instrumentation and Measurement*, **63**, 117-123. <https://doi.org/10.1109/TIM.2013.2277562>
- [3] Shea, J.D., Kosmas, P., Hagness, S.C. and VanVeen, B.D. (2010) Three Dimensional Microwave Imaging of Realistic Numerical Breast Phantoms via a Multiple Frequency Inverse Scattering Technique. *Medical Physics*, **37**, 4210-4226. <https://doi.org/10.1118/1.3443569>

- [4] Kuwahara, Y., Miura, S., Nishina, Y., Mukumoto, K., Ogura, H. and Sakahara, H. (2013) Clinical Setup of Microwave Mammography. *IEICE Transactions on Communications*, **E96.B**, 2553-2562. <https://doi.org/10.1587/transcom.E96.B.2553>
- [5] Ono, Y. and Kuwahara, Y. (2017) Microwave Tomography Assisted by Radar Imaging. *Proceeding of the 2017 47th European Microwave Conference*, Nuremberg, Germany, 10-12 October 2017, 880-883. <https://doi.org/10.23919/EuMC.2017.8230985>
- [6] Paulsen, K.D., Meaney, P.M. and Gilman, L.C. (2006) *Alternative Breast Imaging*, Springer, Boston, MA. <https://doi.org/10.1007/b101336>
- [7] Islam, M.T., Mahmud, M.Z., *et al.* (2019) A Low Cost and Portable Microwave Imaging System for Breast Tumor Detection Using UWB Directional Antenna Array. *Scientific Reports*, **9**, Article No. 15491. <https://doi.org/10.1038/s41598-019-51620-z>
- [8] Klemm, M., Craddock, I.J., *et al.* (2009) Radar-Based Breast Cancer Detection Using a Hemispherical Antenna Array—Experimental Results. *IEEE Transactions on Antennas and Propagation*, **57**, 1692-1704. <https://doi.org/10.1109/TAP.2009.2019856>
- [9] Wang, L. (2019) Multi-Frequency Holographic Microwave Imaging for Breast Lesion Detection. *IEEE Access*, **7**, 83984-83993. <https://doi.org/10.1109/ACCESS.2019.2924334>
- [10] Aminrh, R.K., McCombe, J., Khalatpour, A. and Nikolova, N.K. (2015) Microwave Holography Using Point Spread Functions Measured with Calibration Object. *IEEE Transactions on Instrumentation and Measurement*, **64**, 403-417. <https://doi.org/10.1109/TIM.2014.2347652>
- [11] Flores-Tapia, D., Gabriel, T. and Pistrius, T. (2010) Wavefront Reconstruction Method for Subsurface Radar Imagery Acquired Along Circular and Planar Scan Trajectories. *IEEE Transactions on Aerospace and Electronic Systems*, **46**, 1346-1363. <https://doi.org/10.1109/TAES.2010.5545193>
- [12] Nagaoka, T., Watanabe, S., Sakurai, K., Kunieda, E. and Watanabe, S. (2004) Development of Realistic High-Resolution Whole-Body Voxel Models of Japanese Adult Male and Female of Average Height and Weight and Application of Models to Radio-Frequency Electromagnetic-Field Dosimetry. *Physics in Medicine and Biology*, **49**, 1-15. <https://doi.org/10.1088/0031-9155/49/1/001>